Stability and Robustness of Real Time Pressure Control in Water Distribution Systems

Article *in* Journal of Hydraulic Engineering · March 2020

DOI: 10.1061/(ASCE)HY.1943-7900.0001722

3 authors, including:

Giacomo Galuppini
Massachusetts Institute of Technology
11 PUBLICATIONS **37** CITATIONS

SEE PROFILE

Enrico Creaco
University of Pavia
113 PUBLICATIONS **1,411** CITATIONS

SEE PROFILE

Stability and Robustness of Real Time Pressure Control in Water Distribution Systems

Giacomo Galuppini *[a], Lalo Magni[b], and Enrico Creaco[c]

[a]MSc, Dipartimento di Ingegneria Civile e Architettura, University of Pavia, Pavia 27100, Italy. Email: giacomo.galuppini01@ateneopv.it
[b]Full Professor, Dipartimento di Ingegneria Civile e Architettura, University of Pavia, Pavia 27100, Italy. Email: lalo.magni@unipv.it
[c]Associate Professor, Dipartimento di Ingegneria Civile e Architettura, University of Pavia, Pavia 27100, Italy. Email: creaco@unipv.it

Abstract

This paper deals with the fundamental requirement of stability of Real Time Control algorithms for Water Distribution Systems. Loss of stability may in fact generate strong pressure waves that cause damages to the structure and increase leakage and maintenance costs. In addition, since the system under control is characterised by a complex, nonlinear dynamic behaviour, it is very important to guarantee that stability is preserved even when the Water Distribution System is working very far from its nominal working point. The aim of this work is therefore to apply tools and methodologies of control system theory to analyse both nominal and robust stability of Real Time Control algorithms in a case study framework. This allows quantitative understanding of the cause of possible instability of the control scheme and suggests how to prevent it. Finally, this work proposes a possible way to improve the design of the control algorithms under investigation, to reduce the risk of instability events and, at the same time, reduce the cost of control.

Author keywords: RTC, WDN, Stability, Robustness, PI.

Introduction

Real Time Control (RTC) is widely adopted in Water Distribution Systems (WDS) to reduce leakage (Farley and Trow (2003)) and to extend the lifetime of the infrastructure (Thornton and Lambert (2006); Lambert et al. (2013)). Many different algorithms can be found in the literature (Campisano et al. (2009, 2011, 2016); Ulanicki and Skworcow (2014); Janus and Ulanicki (2017, 2018); Prescott and Ulanicki (2008); Creaco and Franchini (2013); Creaco (2017); Creaco et al. (2017, 2018); Fontana et al. (2017a,b)). Still, in many cases, the issue of stability is not properly considered in the design of the control algorithm, or it is investigated with qualitative issues only (Campisano et al. (2009, 2011, 2016); Creaco and Franchini (2013); Creaco (2017); Creaco et al. (2017, 2018)). Even a very simple WDS represents a complex nonlinear system, whose dynamic behaviour can be heavily dependent on the working point: the stability analysis becomes then a crucial element in the design of RTC. On the practical hand, loss of stability does not just mean that the pressure can not be regulated to the desired value, but also that very large pressure waves can be triggered. Such waves propagate through the pipes of the WDS, with the risk of damaging the structure itself. A formal stability analysis was proposed for the first time in (Ulanicki and Skworcow (2014); Janus and Ulanicki (2018)), where the authors successfully managed to reproduce in simulation the oscillations recorded on a real plant, in the presence of Proportional-Integral-Derivative (PID) algorithms, Pressure Reducing Valves (PRVs) and very low values of the flow. Their valuable analysis suggests that the cause of instability could be found in the nonlinearity of the gain of the process (Ulanicki and Skworcow (2014)). The authors also suggest a nonlinear gain compensator to robustify the design of the algorithm (Janus and Ulanicki (2018)). An instability event is also faced in Galuppini et al. (2019), where the authors tune and test different control algorithm based on simplified dynamic models of the WDS and working at high sampling rate. In particular, the instability occurs while testing a Proportional Integral (PI) controller at very low flow (see Figure 1a for a whole day simulation and Figure 1b for a detail of the oscillations). Since similar algorithms are of current interest (see Fontana et al. (2017a,b) for other

*Corresponding author.

examples), it is important to understand more about stability when PI and PID RTC algorithms are adopted. The aim of this work is then twofold. On one hand, starting from the considerations introduced in Ulanicki and Skworcow (2014) and Janus and Ulanicki (2018) for PRVs and exploiting the tools of control system theory, it aims to perform a detailed and quantitative stability analysis of the PCVs based RTC algorithms proposed in Galuppini et al. (2019), to further clarify the cause of the instability. On the other hand, it aims to propose design tools and methodologies which can help preventing such instability events.

The issue of *robustness* is also investigated. In fact, regardless of what design technique is used for the design, controllers are always designed based on necessary incomplete information about the dynamic behaviour of the process (the model). The accuracy of the model varies but is never perfect. In addition, the dynamic behaviour of the plant may change in time, and such changes are rarely captured in the models. It is most desirable that the controllers is insensitive to this kind of model uncertainty, that is, it should be *robust* (Morari and Zafiriou (1989)). Typically there are two main approaches to consider robustness in control design: robust control and robustness analysis. In the first case, a model of the uncertainty affecting the model of the plant must be known, and the goal is to synthesize a controller that guarantees closed-loop stability for any possible uncertainty described by the considered uncertainty model (Zhou et al. (1986)). In the second case, the synthesis of the controller is based on a nominal model of the plant and on a robustness analysis. In this second case the model of the uncertainty is not expected to be known, and therefore no stability is guaranteed (Magni and Scattolini (2014)). On the other hand, the main drawback of the first approach is the need to provide a model for the uncertainty and, typically, a loss in terms of performance arising from the trade off with the necessity of considering the worst possible uncertainty.
The approach adopted in this work considers only *robustness analysis*, based on local, linear models of the system, identified from simulated experiments performed on the case study WDS. In particular, this work stresses the need for linear models with higher order, to properly describe the unusual high frequency behaviour of the plant, both in the design phase and in the stability and robustness analysis.

The paper is organised as follows: the first section resumes the methodology for the numerical modelling of the WDSs, resumes the procedure for the design of the RTC algorithms and describes the methodology that allows evaluating stability and robustness of the control design. Some important remarks about how stability and robustness benefit from the introduction of a lowpass filter and a Smith Predictor in the design of the RTC algorithm are introduced as well. The second section introduces the details of the case studies and applies the methodology to perform a detailed analysis of stability and robustness of the RTC algorithms. A detailed discussion of results is provided for each case study. Finally, the conclusion section resumes the main contribution of this work. An appendix section is also present to recall some of the concepts of control system theory used in the paper. In particular, the concepts of Laplace transform, transfer function, frequency response, Bode and Nyquist plots are reported.

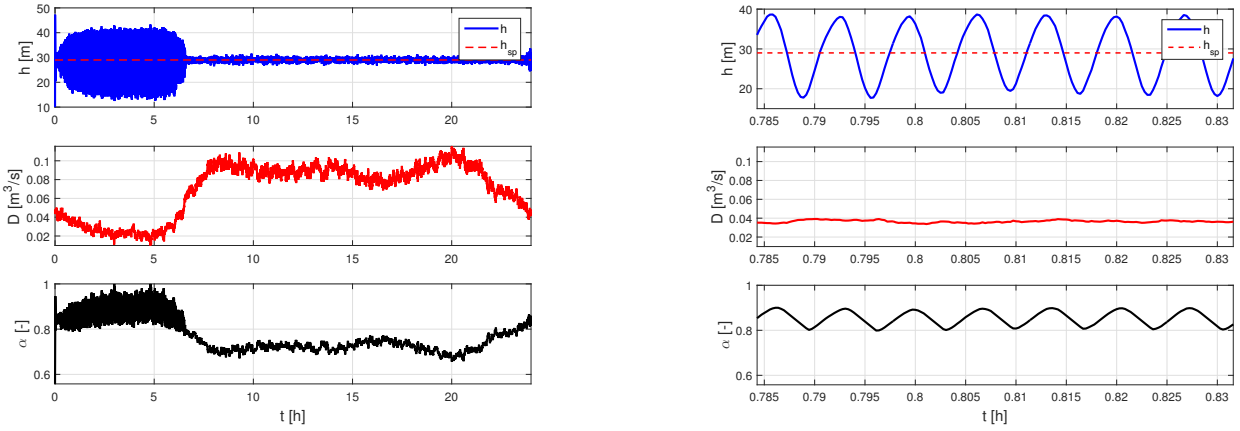

(a) (b)

Figure 1: (a) Closed-loop simulation with PI_{na} algorithm, showing large oscillations at low flow, and (b) detail of the oscillations. Signals: pressure $h(t)$ and pressure setpoint h_{sp}, demand $D(t)$, valve closure $\alpha(t)$.

Methodology

This section is devoted to the description of the theoretical and methodological aspects of this work, at three different levels:

- methodology for the hydrodynamic simulation of the Water Distribution Systems under investigation.
- methodology for the design of the RTC algorithms.
- methodology for the stability and robustness analysis of the proposed RTC algorithms.

Hydrodynamic Simulation

In order to properly consider the effect of hydraulic transients due to rapid nodal demand and/or valve setting variations, the 1D unsteady flow modelling described in Creaco et al. (2017) is used for simulations. Each pipe is discretised with a suitable spatial step. The integration time step is selected according to the spatial discretisation and to the celerity of the pressure wave propagating through the pipe. Total heads and water discharges are calculated at each time step by solving the water hammer partial differential equations with the method of characteristics (Streeter et al. (1998)). Suitable boundary conditions are assigned in correspondence to the source and demanding nodes. The effect of the control valve is modelled by considering no link at the valve site and setting nodal outflow at the upstream end Q_{up} at:

$$Q_{up} = \sqrt{\frac{2g}{\xi(\alpha)}} A \sqrt{\Delta H_{valve}} \tag{1}$$

where g is the gravity acceleration, A is the valve area, ξ is the valve head loss coefficient, ΔH_{valve} is the head drop in the valve and α is the valve closure setting, ranging from 0 (fully open) to 1 (fully closed). The valve head loss coefficient is a growing function of α (Walski et al. (2003)). The inflow at the downstream end Q_{down} is set, instead, at:

$$Q_{down} = Q_{up} \tag{2}$$

For a more complex Water Distribution Network case study, the correction proposed in Pezzinga (2000) is introduced in the modelling, to obtain more careful evaluation of friction slope associated with the unsteady flow. In addition, to obtain a better description of the system dynamics, a pressure driven modelling approach is chosen for the implementation of the WDN simulator, as proposed in Ciaponi et al. (2015). To account for leakage from WDN pipes, the following outflow q is considered:

$$q = \alpha_{leak} h_p^{\gamma} \tag{3}$$

where α_{leak} $[m/s]$ and γ $[-]$ are the leakage coefficient and exponent, respectively, and h_p $[m]$ is the pressure head along the considered pipe.

Model Based Design of PI RTC Algorithms

This section briefly resumes the design methodology for the RTC algorithms proposed in Galuppini et al. (2019), whose goal is the regulation of the measured pressure at a given setpoint h_{sp}, in presence of time varying demand profile. The design of the algorithms is based on three steps:

- definition of a nominal working point;
- collection of input-output data from step response experiments and identification of a linear model, to describe the dynamic behaviour of the system under control in a neighbourhood of the working point;
- design of the regulator transfer function, according to the control requirements and to the process model.

Nominal Working Point

For the definition of the working point, the water distribution system must be treated as a Multi-Input Single-Output (MISO); its input signals are:

- $\alpha(t)$, the valve closure ($[-]$).
- $H(t)$, the source pressure head ($[m]$).
- $D(t)$, the water demand ($[m^3/s]$).

The output is the pressure $h(t)$ measured at the controlled point.

The nominal working point is then defined by the tuple $WP = (\overline{\alpha}, \overline{H}, \overline{D}, \overline{h})$, with $\overline{\alpha}$ the value of α bringing the measured pressure $h(t)$ to the setpoint h_{sp}, when the demand and the source pressure head are fixed at their mean values.

Step Response Experiments and Model Identification

A simple Single-Input Single-Output (SISO) dynamic model relating the variation of the valve closure (the control variable) to the corresponding variation of pressure (the controlled variable) is used for the synthesis of the regulator. Both source pressure head and demand are in fact considered as disturbances acting on the system, with their values fixed at the working point during the design phase. For this purpose, step response experiments are performed as follows: the system is first led to the desired working point. Then a small step variation of α is applied. Variation signals $\delta\alpha(t) = \alpha(t) - \overline{\alpha}$ and $\delta h(t) = h(t) - \overline{h}$ are computed and constitute the identification data. The structure of the local model is chosen according to the behaviour of the step response $\delta\alpha(t)$, and Matlab Identification Toolbox (Ljung (1991)) is used to identify the values of the parameters that provide the best fit between model prediction and identification data. In Galuppini et al. (2019), the model was represented by $G(s)$, a first order transfer function with delay:

$$G(s) = \frac{\mu_g e^{-s\tau_g}}{1 + sT_g} \tag{4}$$

where μ_g is the static gain, τ_g is the delay and T_g is the pole time constant.

The main aim of this paper is instead to demonstrate that the use of linear, local models with higher order allows to properly describe the high frequency behaviour of the plant, which can not be captured by standard, low order models such as the typical first or second order ones. As it will be discussed with two different case studies, the frequency response of the plant shows in fact many resonance peaks at high frequency. This may spoil the results of the stability and robustness analysis based on low order models, if the desired closed-loop bandwidth is too high in frequency.
The higher order models can be obtained from the step response data. In particular, Matlab Identification Toolbox is used to identify the values of the parameters of $\tilde{G}(s)$, a higher order transfer function. The higher order model prediction should better match the high frequency oscillations of the step response of the system.

Design of the Regulator

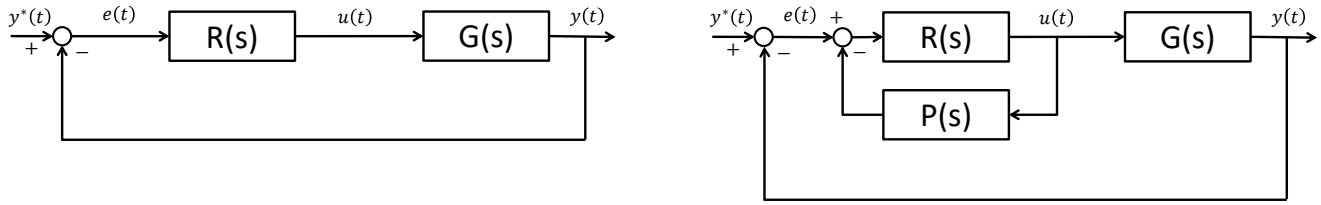

(a) (b)

Figure 2: (a) Block scheme for a negative feedback control loop for linear systems. (b) Block scheme for a negative feedback control loop for linear systems, including the Smith Predictor for delay compensation. In particular, $y(t)$ is the controlled variable, $y^*(t)$ is the reference signal, $e(t) = y^*(t) - y(t)$ is the control error and $u(t)$ is the control variable. $G(s)$ is the process transfer function, $R(s)$ is the regulator transfer function, $P(s)$ is the Smith Predictor transfer function.

This section describes the synthesis of the Proportional-Integral RTC algorithms. Figure 2a depicts the block scheme for general negative feedback control loop for linear systems, where $y(t)$ is the controlled variable, $y^*(t)$ is the reference signal, $e(t) = y^*(t) - y(t)$ is the control error and $u(t)$ is the control variable.
Let $G(s) = Y(s)/U(s)$ be the transfer function describing the dynamics of the process under control, and $R(s) = U(s)/E(s)$ the transfer function of the regulator. In particular, for RTC, $u(t) = \delta\alpha(t)$, $y(t) = \delta h(t)$, $y^*(t) = h_{sp}$, with $G(s)$ obtained from the step response experiment.
The time-domain expression for the PI regulator is (Seborg et al. (2010)):

$$u(t) = K_p e(t) + K_i \int e(t)dt \tag{5}$$

With the application of Laplace transform, it holds that:

$$U(s) = K_p E(s) + \frac{K_i}{s} E(s) \tag{6}$$

Hence, the transfer function of the regulator can be written as follows:

$$R(s) = \frac{U(s)}{E(s)} = K_p + \frac{K_i}{s} = \frac{K_p s + K_i}{s} = K_i \frac{1 + s\frac{K_p}{K_i}}{s} \tag{7}$$

By defining $T_i = \frac{K_p}{K_i}$ and $\mu_r = K_i$, one has:

$$R(s) = \mu_r \frac{1 + sT_i}{s} \tag{8}$$

The design approach originally adopted in Galuppini et al. (2019) is pole compensation: the zero of the regulator is used to compensate for the effect of the slowest pole of the process. This means setting:

$$T_i = T_g \tag{9}$$

Then, it is possible to define:

$$\mu_r = \frac{\omega_c}{\mu_g} \tag{10}$$

where ω_c is the desired closed-loop bandwidth expressed in rad/s.
The resulting loop transfer function $L(s)$ is:

$$L(s) = \frac{\omega_c}{s} e^{-s\tau} \tag{11}$$

where the only free design parameter is ω_c, which has to be tuned with a trial and error procedure.

In this work, different higher order models $\tilde{G}(s)$, describing the process dynamics around different working points, are adopted in order to tune ω_c (i.e. the gain of the regulator) directly on the model, with no need for trial and error procedures on the plant.
The higher order model is also useful to reduce the cost of control by a better analysis of the control sensitivity function.

The regulators are implemented in a discrete time way. Discretisation is performed with Tustin method to ensure that stability properties of $R(s)$ are preserved. The chosen sampling time T_s, must be consistent with Nyquist Sampling Theorem (Seborg et al. (2010)).

Stability and Robust Stability of Linear Feedback Systems

This section is devoted to the introduction of the main stability theorems for feedback linear systems. These results will allow verification of the stability of the RTC algorithms.

The stability of a dynamic system represented by a transfer function can be assessed by computing the roots of its denominator, called poles. In particular, the system is asymptotically stable if and only if all the poles have negative real part (Seborg et al. (2010)). With reference to the general scheme of Figure 2a, let us recall $L(s) = G(s)R(s)$ and define the complementary sensitivity function:

$$F(s) = \frac{Y(s)}{Y^*(s)} = \frac{L(s)}{1 + L(s)} \tag{12}$$

The transfer function $F(s)$ describes the behaviour of the overall feedback system.
Let us assume that no pole with non-negative real part is cancelled while performing the product $G(s)R(s)$. Then, the feedback system is asymptotically stable if and only if all the poles of $F(s)$ have negative real part (Seborg et al. (2010)). From the definition of $F(s)$, this coincides with the study of the roots of $1+L(s)$. This procedure results quite cumbersome during the design of $R(s)$. To simplify it, different tools were developed to study the stability of the closed-loop system from the analysis of the loop function $L(s)$. The *Nyquist criterion* is an useful tool that allows evaluation of the stability of a feedback system, based on the analysis of the Nyquist plot of $L(s)$ (Seborg et al. (2010)). The criterion is reported in the following Theorem.

Theorem 1. *Let Np be the number of poles of $L(s)$ with positive real part, and let N be the number of turns the Nyquist diagram of $L(s)$ makes around the point -1. Each counter-clockwise turn must be counted as positive, while each clockwise turn must be counted as negative. If the Nyquist plot intersects the point -1, then N is not well-defined. Then the negative feedback system is asymptotically stable if and only if N is well defined, and $N = Np$.*

The Nyquist criterion allows evaluating the stability of a linear feedback control scheme in nominal conditions.
However, in practice, it is necessary to account for model uncertainties, in particular when the design is based on a linear,

local approximation of a nonlinear system. The stability analysis must be extended to take into account this "perturbed" framework. Let us consider a *nominally stable* feedback system. Then, if stability holds even in case of heavy uncertainties affecting $L(s)$, the system is said to be *robustly stable*.

A general *robustness* indicator is the *vectorial stability margin*, which can be defined with reference to the Nyquist plot of $L(s)$, as the *minimum distance between the point -1 and the Nyquist plot*. However, the vectorial stability margin can not be straightforwardly applied during the design phase of the loop function $L(s)$. It is therefore helpful to introduce the following indicators, that can be derived from the vectorial stability margin as particular cases:

- *Phase margin*: $\phi_m = 180° - |argL(j\omega_c)|$, with ω_c s.t. $|L(j\omega_c)| = 1$, representing the maximum unmodelled delay admissible in the loop function that does not compromise asymptotic stability.
- *Gain margin*: $K_m = 1/|L(j\omega_\pi)|$, with ω_π s.t. $arg(L(j\omega_\pi)) = -180°$, representing the maximum unmodelled gain admissible in the loop function that does not compromise asymptotic stability.

Both these indicators can be directly evaluated from the Bode or Nyquist diagrams of $L(s)$.

The *Phase margin* indicator can also be useful to prove nominal stability of a feedback system from the analysis of the Bode diagram of $L(s)$, under some preliminary hypotheses: Theorem 2 summarises the *Bode criterion*, typically used to prove stability during the synthesis of regulators (Seborg et al. (2010)) .

Theorem 2. *Let $L(s)$ have poles with non-positive real part only, and let the Bode diagram of $|L(j\omega)|_{dB}$ cross the 0 dB axis only once, from above, at $\omega = \omega_c$. Then, by defining μ_L as the gain of $L(s)$ and as $\phi_m = 180° - |argL(j\omega_c)|$ the phase margin, the negative feedback system is asymptotically stable if and only if $\mu_L > 0$ and $\phi_m > 0$.*

When the higher order model $\tilde{G}(s)$ is available, the stability and robustness analysis is then performed based on $\tilde{L}(s) = R(s)\tilde{G}(s)$, thus allowing a better estimation of the robustness margin of the proposed design and, in case of undesired behaviour, a retuning of the regulator itself, based on a better description of the system dynamics.

Remark: Note that, when the regulators are implemented in a discrete time way, the discretisation introduces a phase margin loss ϕ_d, which must be taken into account in the evaluation of the robustness (Seborg et al. (2010)). The phase margin loss can be computed as follows:

$$\phi_d = -\frac{T_s}{2}\omega_c\frac{180}{\pi} \tag{13}$$

Model Based Design of Filtered PI and Smith Predictor RTC Algorithms

The Filtered-Proportional Integral algorithm with Smith Predictor ($FPI - SP$ algorithm) is characterised by three elements:

- a Proportional-Integral regulator, as discussed in the previous section;
- a low-pass filter with unitary gain;
- a Smith Predictor.

With reference to Figure 2b, the regulator $R(s)$ is the cascade of a PI regulator and the low pass filter given by the transfer function $R_f(s)$, reported in (14).

$$R_f(s) = \frac{(1 + sT_d)}{(1 + sT_f)} \tag{14}$$

with T_d the zero time constant and T_f the pole time constant.

The filtering pole is placed just outside of the closed-loop bandwidth, to keep the Bode diagram of $L(s)$ lower at high frequency. Note that the additional pole reduces the phase margin of the system: the zero of $R_f(s)$ can be used to limit this phase margin loss. The phase margin is instead enhanced by the introduction of the Smith Predictor, represented by the transfer function $P(s)$. The system under control is in fact characterised by the presence of a pure delay $e^{-s\tau}$, whose effect is a reduction of the phase margin by a factor:

$$\phi_\tau = -\tau\omega_c\frac{180°}{\pi} \tag{15}$$

with τ the delay expressed in *seconds*.

The aim of the Smith Predictor is to compensate the effect of the delay Seborg et al. (2010). In particular, let:

$$G(s) = G'(s)e^{-s\tau} \tag{16}$$

where $G'(s)$ is a rational transfer function. Then it is possible to neglect the presence of the pure delay $e^{-s\tau}$ in the design of the regulator $R(s)$ by setting:

$$P(s) = (1 - e^{-s\tau})G'(s) \tag{17}$$

Remark: In presence of the Smith Predictor, according to Figure 2b, the loop function $L(s)$ must be computed as:

$$L(s) = G(s)\frac{R(s)}{1 + P(s)R(s)} = G(s)R'(s) \tag{18}$$

with:

$$R'(s) = \frac{R(s)}{1 + P(s)R(s)} \tag{19}$$

Case Studies

This work focuses on two different case studies: a Water Distribution System characterised by a simple topology (depicted in Figure 3a), and the skeletonized layout of a real Water Distribution Network (depicted in Figure 4). The details of the two case studies are reported in this section.

Water Distribution System

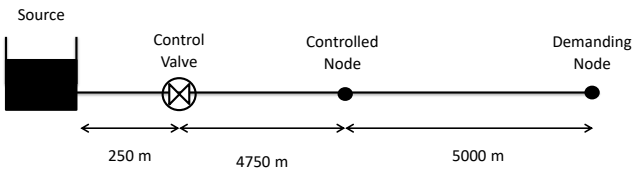

(a)

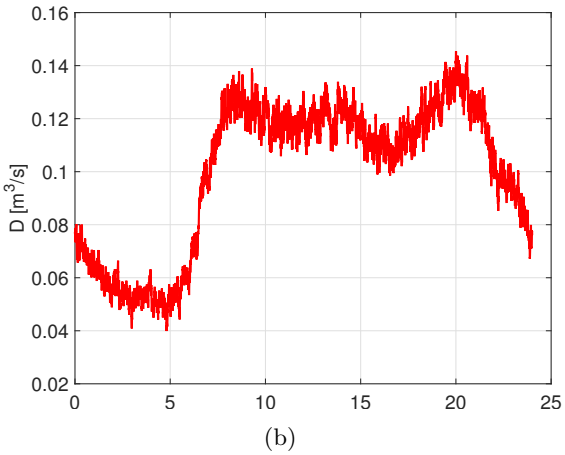

(b)

Figure 3: (a) Topology of the water distribution system. (b) Nominal demand profile.

The Water Distribution System under investigation is characterised by a source node, and a pipe connecting it to a single demanding node, placed 10000 m downstream of the source node. The topology of the water distribution system and the time behaviour of the demand are depicted in Figures 3a and 3b. The source node provides a constant pressure of 50 m. The demand profiles is generated according to the statistic model proposed in Creaco et al. (2017). Different offsets, ranging in the interval $[-0.03; +0.05\ m^3/s]$, are added to the main demand profile to perform tests at very low or very high flow. No leakage is considered in this setup for simplification purposes. A pressure control valve (PCV) is installed 250 m downstream from the source node. In this particular case study, the PCV characteristic curve is given by:

$$\xi(\alpha) = 10^{1.5 - 2.8log_{10}(1-\alpha)} \tag{20}$$

as described in Campisano et al. (2011). A pressure sensor is placed in the middle of the pipe (5000 m downstream from the source node), providing real time measures for control purposes.

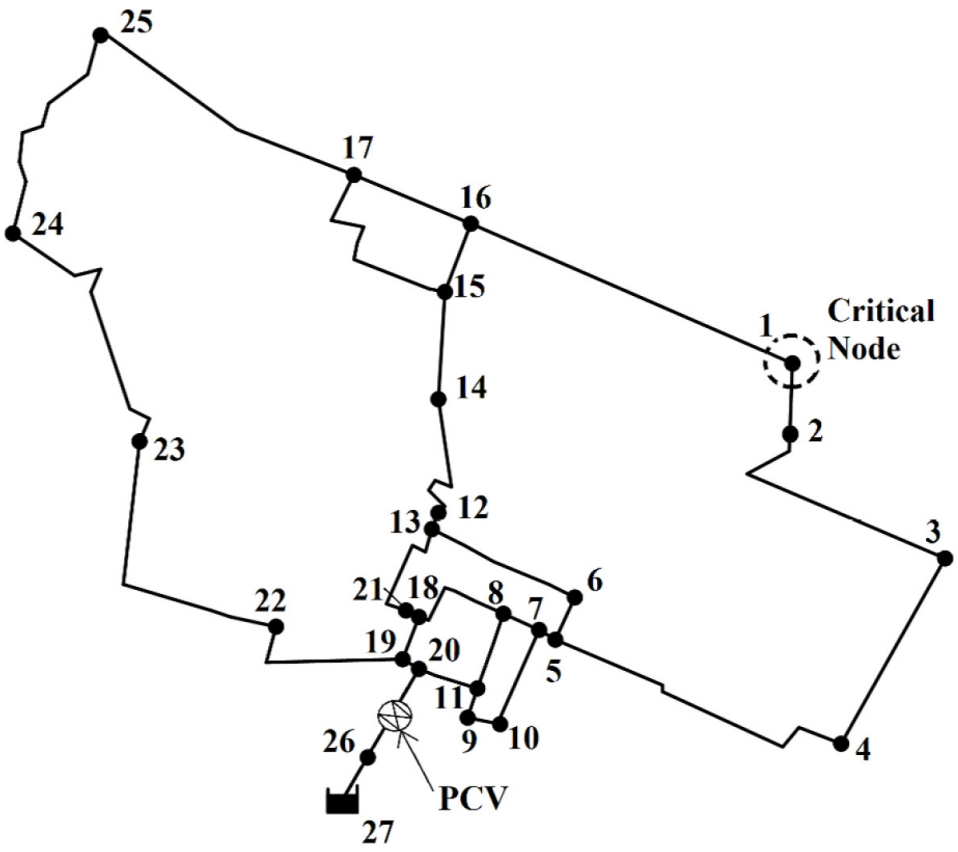

Figure 4: Topology of the WDN

Note that, due to its simple topology, the dynamic behaviour of this system is mainly determined by the water hammer effect. Its impact in case of RTC implemented with short sampling times must be carefully considered in order to avoid instability problems (Janus and Ulanicki (2017); Ulanicki and Skworcow (2014)).

Remark. The maximum actuator speed was initially limited to 0.01 s^{-1} in Galuppini et al. (2019). Since this speed saturation could in principle be a cause of oscillation, the simulation reported in Figure 1a was repeated without limiting the actuator speed, to highlight that the oscillations here reported are not a consequence of such saturation.

PI RTC algorithms

The methodology reported above is now applied step by step to the case study to tune a PI regulator. The first step of the procedure is the definition of the nominal working point, related to the desired pressure setpoint $\overline{h} = 29\ m$. The nominal working point results:

$$WP = \begin{cases} \overline{\alpha} = 0.694 \\ \overline{H} = 50\ m \\ \overline{D} = 0.1\ m^3/s \\ \overline{h} = 29\ m \end{cases} \tag{21}$$

The procedure then requires application of step response variations of the control variable α, and to record the corresponding variations of the controlled variable h, to be used as identification data for the linear model. The shape of the step response suggests the choice for the process model of a first order transfer function with delay, which results:

$$\begin{gathered} G_{ah}(s) = \frac{\mu_g e^{-s\tau_g}}{1+sT_g} \\ \mu_g = -107.27\ m \quad T_g = 16\ \text{s} \quad \tau_g = 11\ \text{s} \end{gathered} \tag{22}$$

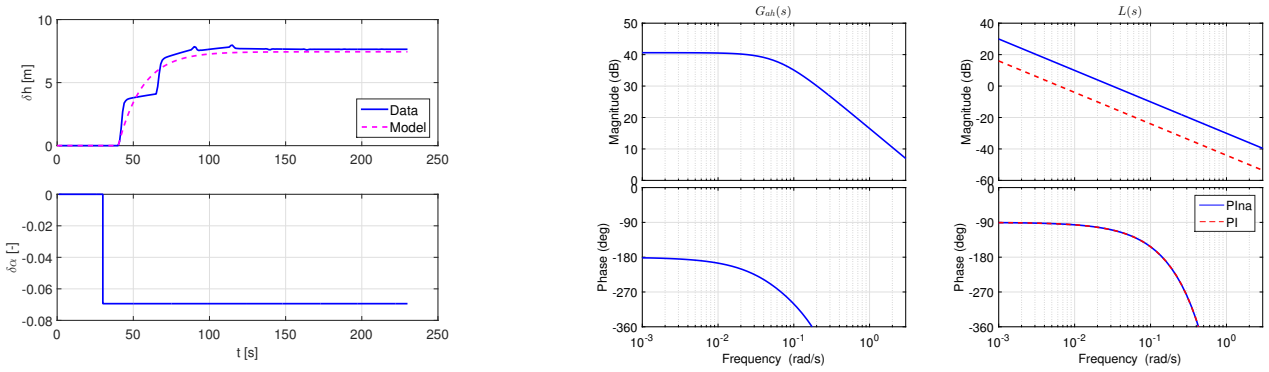

(a) (b)

Figure 5: (a) Step response identification data and model prediction. Signals: measured (solid line) and predicted (dashed line) pressure variation $\delta h(t)$, valve variation $\delta\alpha(t)$. (b) Bode diagram of $G_{ah}(s)$, Bode diagram of $L(s)$ with PI_{na} algorithm (solid line) and Bode diagram of $L(s)$ with PI algorithm (dashed line).

where $G_{ah}(s)$ is a transfer function in the Laplace domain. The step response data and the pressure time evolution predicted by the model are reported in Figure 5a. The Bode diagram of $G_{ah}(s)$ is depicted in Figure 5b.

The last step of the procedure is the design of the regulator, based on the linear model. The synthesis is performed according the model introduced in Equation (22) and the procedure based on pole cancellation. Let this regulator be referred to as PI_{na} algorithm. The resulting loop function is denoted as $L_{PIna}(s)$, and is given by:

$$L_{PIna}(s) = \frac{0.0314}{s} e^{-11s} \tag{23}$$

The Bode diagram of $L_{PIna}(s)$ is depicted in Figure 5b. The regulator is implemented in a discrete time way. Discretisation is performed with Tustin method to ensure that stability properties of $R(s)$ are preserved. The chosen sampling time is $T_s = 1$ s, which is consistent with Nyquist Sampling Theorem (Seborg et al. (2010)).

Stability of PI RTC Algorithms in Nominal Conditions

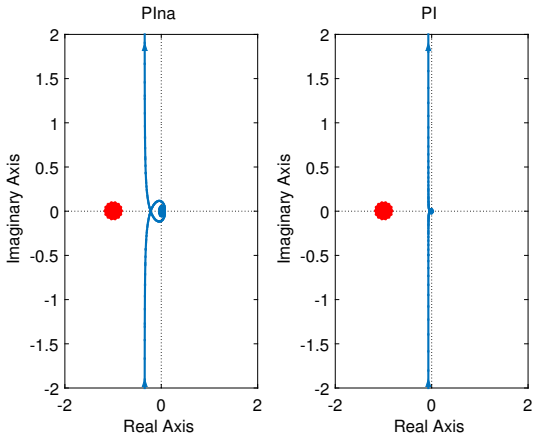

Figure 6: Nyquist diagrams of $L(s)$ with PI_{na} algorithm and PI algorithm.

The stability analysis of the PI_{na} algorithms is now performed exploiting the above stability criteria. The PI_{na} algorithm results in the loop function reported in (23), with $\omega_c = 0.0314\ rad/s$ and phase margin $\phi_m = 70°$. The phase margin loss associated to the discretisation results $\phi_d = -0.9\ °$. The Bode diagram of $L_{PIna}(s)$ is reported in Figure 5b. Is is straightforward to verify that the hypotheses required for the application of Bode criterion are fulfilled. Therefore, since $\phi_m > 0$ and $\mu_L > 0$, the feedback system is asymptotically stable. The stability analysis can be also performed by relying on the Nyquist diagrams of the loop function $L_{PIna}(s)$, which is depicted in Figure 6. Note that the point -1 is not encircled by the Nyquist plot ($N = 0$), and $N_p = 0$, therefore asymptotic stability can be concluded since $N = N_p$.

	Control algorithm	
Robustness indicator	*PInа*	*PI*
ϕ_m	70°	86°
K_m	4.6	22.6

Table 1: Robustness indicators for the PI_{na} and PI RTC algorithms based on $L(s)$.

	Control algorithm	
Robustness indicator	*PInа*	*PI*
ϕ_m	59.5°	80.6°
K_m	1.9	9.5

Table 2: Robustness indicators for the PI_{na} and PI RTC algorithms based on $\tilde{L}(s)$.

When the proposed tuning is applied to the plant, it performs well for nominal demand profile or higher mean values, but becomes unstable and introduces large oscillations when the demand drops to lower values, as reported in Figures 1a and 1b (details of the simulations are available in Galuppini et al. (2019)). Note that the stability analysis performed above is based on a *model* of the system, which is by definition an approximation of the real process. In particular, as shown in Figure 5a, the linear model $G_{ah}(s)$ only provides a low frequency approximation of the dynamics of the system. Moreover, due to the nonlinearity of the process under control, such linear model is only valid locally, in a neighbourhood of the working point. Consequently, the stability results here obtained hold in such neighbourhood only. This is particularly interesting since the simulations show that the PI_{na} algorithm becomes unstable with very low values of the flow through the pipe (that is when the system moves very far from the nominal working point).

In order to extend the stability analysis and quantitatively understand the cause of the recorder instability, the robustness indicators are now evaluated and the analysis repeated around the working point characterised by low flow.

Robust Stability of PI RTC Algorithms

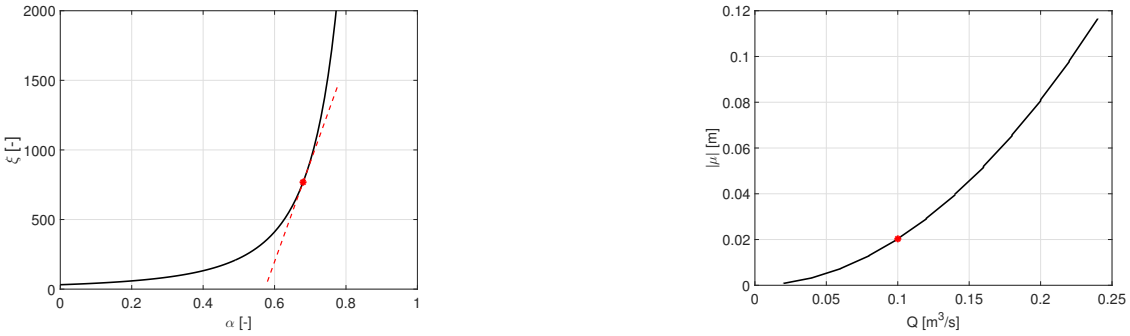

(a) (b)

Figure 7: (a) The local loss coefficient ξ as function of the valve closure α and the straight line tangent to the curve in the working point. (b) Absolute value of the gain of the linearised system μ as function of the flow Q.

The phase and gain margins are now evaluated for the PI_{na} tuning. Results are reported in Table 1. In particular, in this section, focus is put on the gain margin, which is expected to play an important role since some known nonlinearities affecting the system are related to the gain of $G_{ah}(s)$ (Galuppini et al. (2019); Creaco and Franchini (2013); Janus and Ulanicki (2018, 2017); Prescott and Ulanicki (2008)). In particular, focusing on (1), α does not directly affect the pressure loss, but appears through ξ. The relation between ξ and α is strongly nonlinear, as apparent from Figure 7a. Moreover, the absolute value of the gain increases with the square of the flow, as depicted in Figure 7b. The relation is obtained by repeating the identification procedure at different flow values, maintaining the value of $\overline{\alpha}$ and the step amplitudes unchanged.

Nevertheless, in a closed-loop framwork, the two nonlinearities do not cumulate, but are likely to compensate: in case of an increase in the flow, a decrease in the pressure h occurs. The valve closure α must then decrease to compensate for the pressure loss. An increase in the flow, that is an increase in the gain, then results in a decrease in α, that is a decrease in the gain. The same reasoning can be applied in case of a decrease in the flow. In addition, the gain margin provided by

the PI_{na} algorithms seems to be quite large. Therefore, it is still not clear if and how the aforementioned nonlinearities can result in the instability of the feedback system.

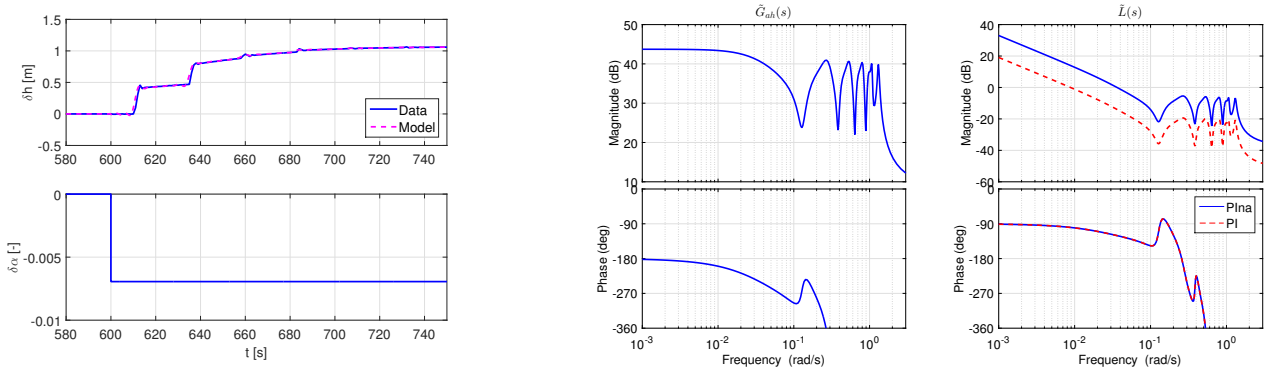

(a) (b)

Figure 8: (a) Step response identification data and model prediction from $\tilde{G}_{ah}(s)$. Signals: measured (solid line) and predicted (dashed line) pressure variation $\delta h(t)$, valve variation $\delta\alpha(t)$. (b) Bode diagram of $\tilde{G}_{ah}(s)$, Bode diagram of $\tilde{L}(s)$ with PI_{na} algorithm (solid line) and Bode diagram of $\tilde{L}(s)$ with PI algorithm (dashed line).

PI Gain Design Based on Higher Order Models

To better understand the cause of the instability of the PI_{na} algorithm, a more accurate local model for the system under control is identified from the step response data, to obtain a better approximation of $L(s)$ around the working point. Figure 8a shows the identification data and the output predicted by $\tilde{G}_{ah}(s)$, a transfer function of higher order, whose parameters are identified from the data by means of Matlab Identification Toolbox. Note how the model prediction now closely follows the time evolution of the pressure.
Figure 8b shows the Bode diagram for $\tilde{G}_{ah}(s)$. A comparison of the Bode diagrams of $G_{ah}(s)$ and $\tilde{G}_{ah}(s)$ (respectively Figure 5b and 8b) highlights in $\tilde{G}_{ah}(s)$ the presence of a number of resonance peaks at high frequency. This behaviour can not be captured by the simpler first order transfer function $G_{ah}(s)$, which instead decreases with slope -20dB/decade. Let us now analyse the Bode diagrams of the loop function, $\tilde{L}_{PIna}(s)$, obtained applying the PI regulator to $\tilde{G}_{ah}(s)$, as in Figure 8b. The hypotheses for the application of Bode criterion are fulfilled: $\mu_L > 0$ and $\phi_m > 0$, therefore asymptotic stability can again be concluded around the nominal working point.
The robustness indicators obtained from $\tilde{L}_{PIna}(s)$ are reported in Table 2. Note that, while the phase margin was just slightly overestimated, the gain margin is strongly overestimated by the simpler G_{ah} model. This is due to the presence of the resonance peaks, which bring the Bode diagram of $\tilde{L}(s)$ much closer to the 0 dB axis than expected.

The last step of this analysis consists in repeating the procedure at a different working point, characterised by very low flow and very high values of α. These are the conditions that bring PI_{na} to instability. In particular, let define the low flow working point WP^{lf}:

$$WP^{lf} = \begin{cases} \overline{\alpha} = 0.88 \\ \overline{H} = 50\ m \\ \overline{D} = 0.03\ m^3/s \\ \overline{h} = 29\ m \end{cases} \tag{24}$$

The step response identification data, obtained performing the simulated experiment around WP^{lf}, are reported in Figure 9a. The same Figure shows also the model prediction obtained from $\tilde{G}^{lf}_{ah}(s)$, again a transfer function of higher order. Figure 9b shows the Bode diagrams of $\tilde{G}^{lf}_{ah}(s)$ and highlights that both the static gain and the height of resonance peaks have increased, with respect to $\tilde{G}_{ah}(s)$.
Let now try to verify stability from the analysis of the Bode diagrams of the loop function $\tilde{L}^{lf}(s)$ (see Figure 9b). Note that the Bode diagram of $\tilde{L}^{lf}_{PIna}(s)$ is now crossing the 0 dB axis many times. The Bode criterion can not be applied to prove stability. In order to draw some conclusions about the stability of the PI_{na} algorithm, it is necessary to rely on the Nyquist plot of $\tilde{L}^{lf}_{PIna}(s)$, which is depicted in Figure 10. Note that, in this case, the point -1 is encircled many times by

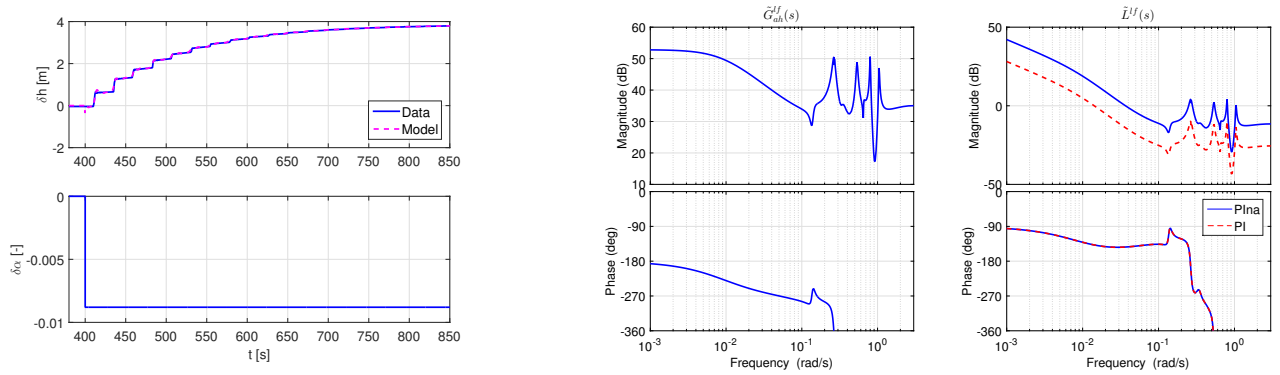

(a) (b)

Figure 9: (a) Step response identification data and model prediction from $\tilde{G}^{lf}_{ah}(s)$. Signals: measured (solid line) and predicted (dashed line) pressure variation $\delta h(t)$, valve variation $\delta\alpha(t)$. (b) Bode diagram of $\tilde{G}^{lf}_{ah}(s)$, Bode diagram of $\tilde{L}^{lf}(s)$ with PI_{na} algorithm (solid line) and Bode diagram of $\tilde{L}^{lf}(s)$ with PI algorithm (dashed line).

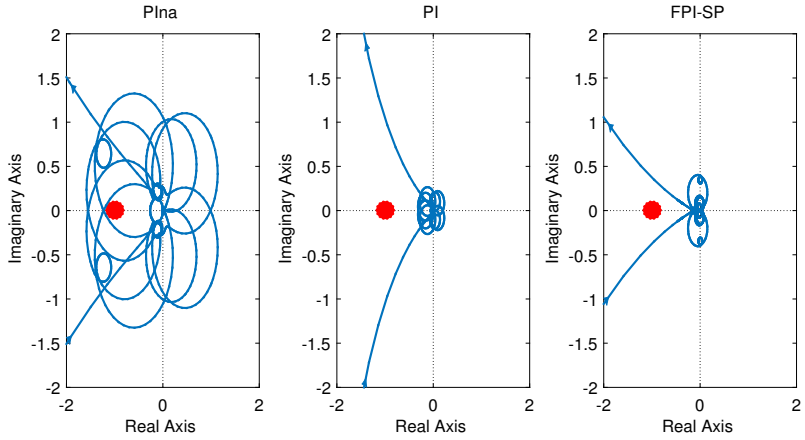

Figure 10: Nyquist diagrams of $\tilde{L}^{lf}(s)$ with PI_{na} algorithm, PI algorithm and $FPI-SP$ algorithm.

the Nyquist plot, while $Np = 0$, therefore the feedback system is unstable, explaining the large oscillations which arise in the low flow simulations.
The whole day trial is shown in Figure 1a, while a detail of the oscillations reported in Figure 1b. Note that the period of the oscillation ($T_w = 25\ s$) is consistent with the frequency of the more pronounced resonance peak of $\tilde{G}^{lf}_{ah}(s)$ (and $\tilde{L}^{lf}_{PIna}(s)$), which is located around $0.26\ rad/s$.

The stability analysis performed above suggests that instability may arise from an increase in the gain of the process, combined with the presence of multiple resonance peaks. The first order model can not capture this phenomenon, and the design of regulator based on such model results inaccurate. In particular, the gain of the regulator has to be tuned with a trial and error procedure. However, the same analysis suggests that the higher order models can be useful tools in the design of the regulator gain, allowing to avoid the trial and error procedure. This section proposes an example of retuning of the PI_{na} algorithm, based on the higher order models. Let this new tuning be referred to as PI algorithm, with the loop function $L_{PI}(s)$ given by:

$$L_{PI}(s) = \frac{0.0063}{s} e^{-11s} \tag{25}$$

with $\omega_c = 0.0063\ rad/s$ and phase margin $\phi_m = 86°$. The Bode diagrams of $L_{PI}(s)$ is depicted in Figure 5b. Note that the new loop function only differs from the old one in the closed-loop bandwidth, which is higher in the $PI_{na}(s)$ case.

This new ω_c was chosen by verifying stability and robustness using the higher order models identified before, around both WP and WP^{lf}. Figure 8b shows the Bode diagram for $\tilde{G}_{ah}(s)$ and the Bode diagrams of the loop function $\tilde{L}_{PI}(s)$ associated to WP. The hypotheses for the application of Bode criterion are fulfilled, since $\mu_L > 0$ and $\phi_m > 0$, and asymptotic stability can again be concluded around the nominal working point. The robustness indicators obtained from

$\tilde{L}_{PI}(s)$ are reported in Table 2. Note how the gain margin is increased by the gain reduction, and how the distance between resonance peaks and the 0 dB axis is increased.
Let now consider the low flow working point WP^{lf}, and the associated higher order model $\tilde{G}_{ah}^{lf}(s)$, whose Bode diagrams are reported in Figure 9a. The same Figure also shows the Bode diagrams of the corresponding loop function $\tilde{L}_{PI}^{lf}(s)$, obtained with the application of the new PI algorithm. The Bode diagram fulfils the hypotheses of Bode criterion, which can be successfully applied to prove asymptotic stability of the feedback system.
Figure 10 also shows the Nyquist diagram for $\tilde{L}_{PI}^{lf}(s)$, which is still far from encircling the point -1, thus providing again some degree of robustness.

When applied to the plant, the new PI algorithm delivers satisfactory results, without any stability issue in all the simulated scenarios (for details of the simulations, see Galuppini et al. (2019)).

Remark. Let consider the stability analysis of the PI algorithm in nominal conditions, based on the nominal first order model. Figure 5b shows the loop function $L_{PI}(s)$. The phase margin results $\phi_m = 86°$, while the phase margin loss associated to the discretisation results $\phi_d = -0.18$ °. The Bode criterion can again be applied to prove the asymptotic stability of the feedback system. The same result can be achieved by means on Nyquist criterion. Figure 6 shows the Nyquist diagrams of the loop function. The point -1 is not encircled by the Nyquist plots ($N = 0$), and $N_p = 0$, therefore asymptotic stability can be concluded since $N = N_p$.
Let now focus on the robustness indicators evaluated in the nominal case, with the first order model: Table 1 highlights the increase in the gain margin, with respect to the previous tuning. A comparison with Table 2 (robustness indicators evaluated with the higher order model) again stresses how the analysis based on the first order model heavily overestimates the gain margin provided by the closed-loop system.

Discussion of Results

The analysis of stability and robustness of the Proportional Integral RTC algorithms performed in the previous sections allows making some remarks:

- The instability of a nominally stable RTC algorithm can be caused by the combined action of the gain nonlinearities and the high frequency resonance peaks of the process.
- A low order model as $G_{ah}(s)$ can not capture such high frequency resonant behaviour, while a higher order model like $\tilde{G}_{ah}(s)$ may provide a better description of the dynamics of water distribution system.When a higher order model is available, the tuning of the regulators can be successfully performed on the model, with no need for trial and error procedures. Still, in some real experimental scenarios, it may be difficult to obtain an accurate higher order model.
- For these reasons, when based on a low order model, the RTC algorithm must be tuned so that *both* phase and gain margin provide a wide degree of robustness to the design, or consider the vectorial stability margin.
- In addition, due to the nonlinearity of the process under control, it is important to verify stability and robustness of the control design around different working points, characterised by very different flow conditions.
- Both Bode and Nyquist diagrams can be useful tools to analyse stability and evaluate robustness of the control design.

In addition, the authors show in Galuppini et al. (2019) that it is possible to improve the design of the Proportional Integral algorithm by introducing a Filtering action and a Smith Predictor. These elements were originally introduced to filter high frequency harmonics and reduce the cost of control as the cumulative motion of the PCV. Still, the stability analysis performed in this work highlights that robustness is also enhanced by this new design, as discussed in the following section.

Improving Robustness and Cost of Control with FPI-SP RTC algorithms

This section highlights how stability and robustness could benefit from the introduction of a lowpass filter and a Smith Predictor in the design of the RTC algorithm. In addition, an detailed explanation of how this design allows to reduce the cost of control is given, based on the same higher order model used for the stability analysis.

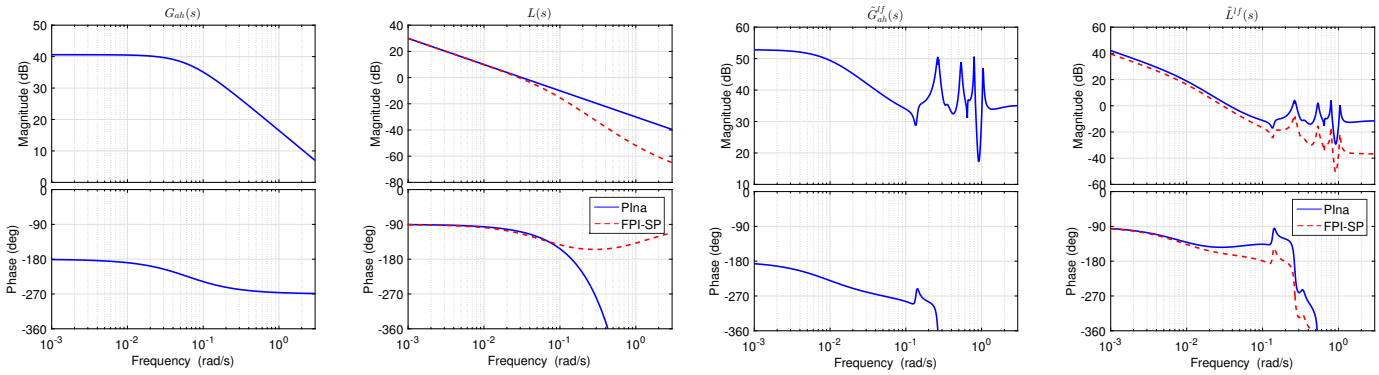

(a) (b)

Figure 11: (a) Bode diagram of $G_{ah}(s)$, Bode diagram of $L(s)$ with PI_{na} algorithm (solid line) and Bode diagram of $L(s)$ with $FPI-SP$ algorithm (dashed line). (b) Bode diagram of $\tilde{G}^{lf}_{ah}(s)$, Bode diagram of $\tilde{L}^{lf}(s)$ with PI_{na} algorithm (solid line) and Bode diagram of $\tilde{L}^{lf}(s)$ with $FPI-SP$ algorithm (dashed line).

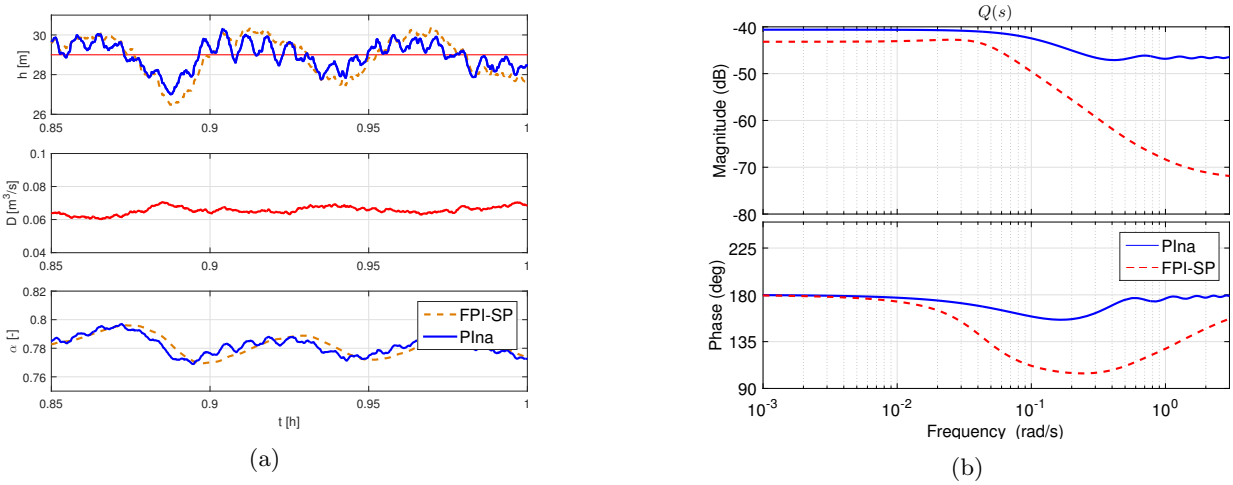

(a) (b)

Figure 12: (a) Closed-loop simulation with $PIna$ (solid line) and $FPI-SP$ (dashed line) algorithms. Signals: pressure $h(t)$ and pressure setpoint h_{sp}, demand $D(t)$, valve closure $\alpha(t)$. (b) Control sensitivity functions for the $PIna$ (solid line) and $FPI-SP$ (dashed line) algorithms.

Design of the Regulator

The PI_{na} algorithm previously introduced is extended with the Smith Predictor based on $G_{ah}(s)$, and the low-pass filter tuned as follows:

$$T_d = \frac{1}{5}\frac{T_w}{2\pi} \quad T_f = 20T_d \tag{26}$$

The resulting loop function $L_{FPI-SP}(s)$, based on $G_{ah}(s)$ and assuming that the effect of the delay is correctly compensated, is depicted in Figure 11a. The regulator is implemented in a discrete time way. Discretisation is performed with Tustin method to ensure that stability properties of $R(s)$ are preserved. The chosen sampling time is 1 s, which is consistent with Nyquist Sampling Theorem (Seborg et al. (2010)).

Stability analysis of FPI-SP RTC Algorithm

Stability and Robustness of $FPI-SP$ algorithm are now evaluated according to the procedure introduced in this work. The nominal stability can be proven by means of the Bode criterion, since $\mu_L > 0$ and $\phi_m = 67° > 0$. In addition, one has $K_m = \infty$, since the phase of $L_{FPI-SP}(s)$ never reaches $-180°$. The phase margin loss associated to the discretisation results $\phi_d = -0.9\ °$. In comparison to the PI_{na} algorithm, it is possible to note that the gain margin is heavily increased, while maintaining the phase margin and ω_c almost unchanged.

From a practical point of view this means that the robustness of the algorithm is increased without reducing the bandwidth of the closed-loop, which in turns impacts on the regulation performances, as instead happened for the PI algorithm. The last step is repeating the analysis around WP^{lf}, to prove stability at low flows. Let $\tilde{L}^{lf}_{FPI_SP}(s)$ be the loop transfer function, obtained from the application of the $FPI-SP$ algorithm to the higher order model $\tilde{G}^{lf}_{ah}(s)$; its Bode diagram is reported in Figure 11b. Note that, while the critical frequency ω_c is almost coinciding for both PI_{na} and $FPI-SP$ algorithm, it is still possible to prove stability of $FPI-SP$ by means of Bode criterion, since the resonance peaks which cause instability of PI_{na} are not crossing the 0 dB axis. In addition, some robustness margin is left to face further variations of the process model. The same result can be obtained from the inspection of the Nyquist plot (see Figure 10), and the application of the Nyquist theorem.

Remark: Note that the loop functions reported in Figure 11a slightly differ in the static gain. This is due to the presence in $FPI-SP$ of the Smith Predictor based on the nominal process model $G_{ah}(s)$, whose static gain is in turn different from that of $\tilde{G}^{lf}_{ah}(s)$.

Cost of Control of FPI-SP RTC Algorithm

The authors already demonstrated in Galuppini et al. (2019) that the algorithm benefits from the new elements in terms of cost of control, evaluated as the overall motion of the PCV during the trial. The filtering action in the regulator transfer function improves rejection of high frequency harmonics of the error signal. This means that the regulator does not try to compensate them, reducing the required motion of the valve, as shown in Figure 12a. This effect can be considered during the design phase by addressing the *control sensitivity function*, which can be defined, with reference to the block diagram of Figure 2a, as:

$$Q(s) = \frac{U(s)}{Y^*(s)} = \frac{R(s)}{1+L(s)} \tag{27}$$

In case of Smith Predictor, it is defined as:

$$Q(s) = \frac{U(s)}{Y^*(s)} = \frac{R'(s)}{1+L(s)} \tag{28}$$

with $R'(s)$ defined according to Equation (19), and $L(s)$ according to Equation (18).
A comparison of the control sensitivity functions associated to the PI_{na} and $FPI-SP$ algorithms is presented in Figure 12b. The two transfer functions are computed with $G(s) = G_{ah}(s)$. Note that the $FPI-SP$ algorithm shows a reduced control sensitivity at high frequency with respect to the PI_{na} algorithm.

Water Distribution Network

The aim of this section is to show that the analysis proposed in this work can also be applied to WDNs with a complex topology. The topology of the skeletonised Water Distribution Network example used to test the RTC algorithms is reported in Figure 4. The network is made up of 26 demanding nodes and 1 source node with ground level of 35 m a.s.l. and an average daily head of 40 m) and 32 pipes. All the network nodes feature a ground elevation of 0 m a.s.l.. Pipe diameters range from 100 mm to 450 mm. The critical node with the lowest pressure head is node 1. Further details about the WDN topology and numerical model can be found in Creaco et al. (2018); Galuppini et al. (2019).

Stability and Robustness Analysis

	Control algorithm	
Robustness indicator	PI	$FPI-SP$
ϕ_m	56.5°	64.5°
K_m	1.15	2

Table 3: WDN: robustness indicators for the PI and $FPI-SP$ RTC algorithms based on $\tilde{L}(s)$.

According to the proposed design procedure, a step response experiment, performed in nominal conditions, leads to the following local model:

$$G_{ah}(s) = \frac{-74.7e^{-18s}}{(1+14.4s)} \tag{29}$$

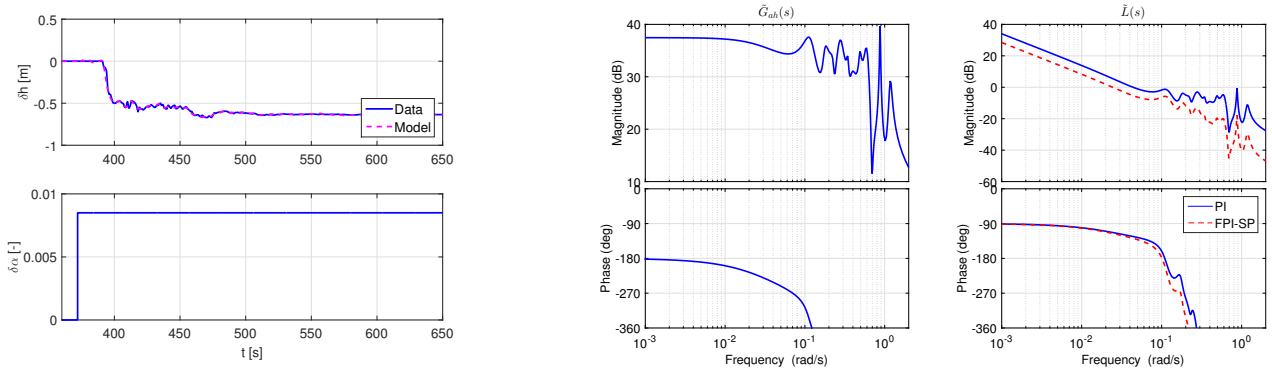

(a) (b)

Figure 13: WDN: (a) Step response identification data and model prediction from $\tilde{G}_{ah}(s)$. Signals: measured (solid line) and predicted (dashed line) pressure variation $\delta h(t)$, valve variation $\delta\alpha(t)$. (b) Bode diagram of $\tilde{G}_{ah}(s)$, Bode diagram of $\tilde{L}(s)$ with PI algorithm (solid line) and Bode diagram of $\tilde{L}(s)$ with $FPI-SP$ algorithm (dashed line).

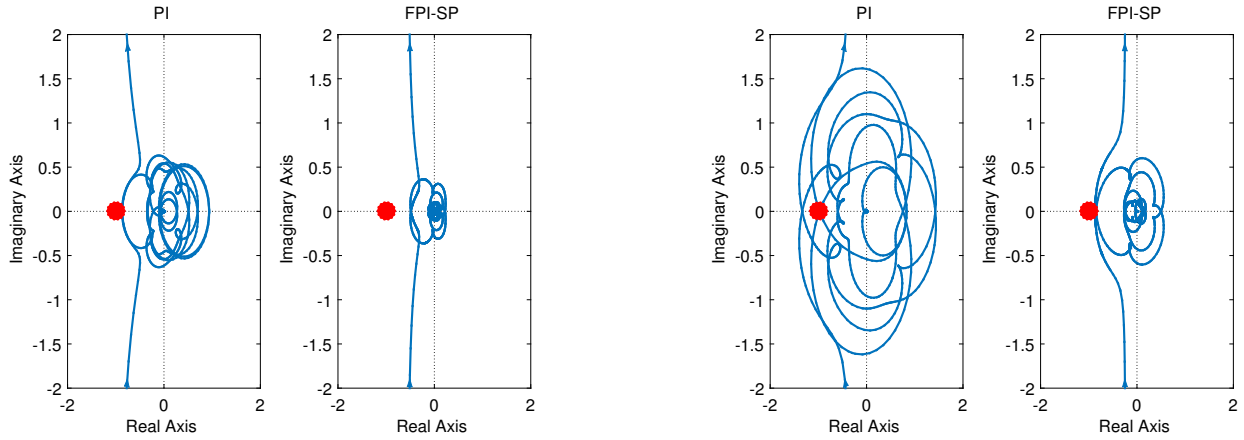

(a) (b)

Figure 14: WDN: (a) Nyquist diagrams of $\tilde{L}(s)$ with PI algorithm and $FPI-SP$ algorithm. (b) Nyquist diagrams of $\tilde{L}^{hf}(s)$ with PI algorithm and $FPI-SP$ algorithm.

A possible tuning for the PI algorithm is then:

$$R_{PI}(s) = \frac{0.00067(1+14.4s)}{s} \tag{30}$$

A possible $FPI-SP$ extension is instead:

$$R_{FPI}(s) = \frac{0.00067(1+14.4s)}{s}\frac{1+1.25s}{1+12.5s} \tag{31}$$

with the Smith Predictor based on $G_{ah}(s)$. The two regulators are implemented in a discrete time way. Discretisation is performed with Tustin method to ensure that stability properties of $R(s)$ are preserved. The chosen sampling time is 1 s, which is consistent with Nyquist Sampling Theorem (Seborg et al. (2010)). The phase margin loss associated to the discretisation results $\phi_d = -1.44\,^\circ$ for both algorithms.

The stability analysis here reported is based on the identification of the higher order model $\tilde{G}_{ah}(s)$ from the same step response experiment used to identify $G_{ah}(s)$. The identification data and the model prediction are reported in Figure 13a. The Bode diagram of $\tilde{G}_{ah}(s)$ is depicted in Figure 13b. Note that high frequency resonance peaks are present also in this case, with even lower damping than in the WDS case. This makes the peaks even more pronounced, with a magnitude of the Bode diagram that is higher than that of the static gain of the transfer function itself, despite a more accurate pressure-driven modelling of the WDN (as suggested in Pezzinga (2000) and Ciaponi et al. (2015)). The same Figure also shows the Bode diagrams of $\tilde{L}(s)$ obtained with the application of the PI and $FPI-SP$ algorithms proposed

above. Stability can be proven with Bode criterion, and, again, note how the $FPI-SP$ algorithm manages to improve the filtering of high frequency harmonics and increase the gain margin, with no significant reduction of the closed-loop bandwidth or phase margin reduction. Figure 14a shows the Nyquist plot for the two algorithms, to highlight their overall robustness as distance from the point -1. Note how the PI algorithm is dangerously close to the point -1, while $FPI-SP$ provides more robustness.

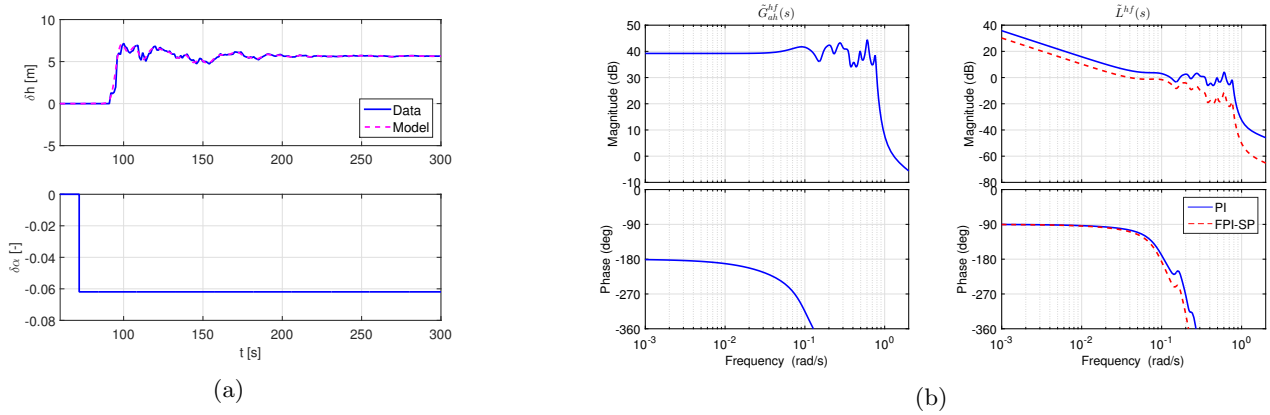

(a) (b)

Figure 15: WDN: (a) Step response identification data and model prediction from $\tilde{G}_{ah}^{hf}(s)$. Signals: measured (solid line) and predicted (dashed line) pressure variation $\delta h(t)$, valve variation $\delta\alpha(t)$. (b) Bode diagram of $\tilde{G}_{ah}^{hf}(s)$, Bode diagram of $\tilde{L}^{hf}(s)$ with PI algorithm (solid line) and Bode diagram of $\tilde{L}^{hf}(s)$ with $FPI-SP$ algorithm (dashed line).

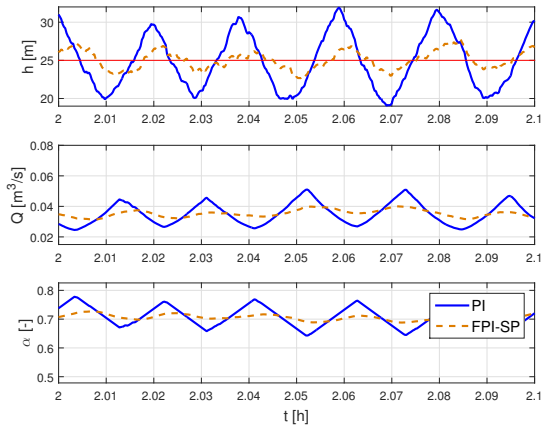

Figure 16: WDN: Closed-loop simulation with PI (solid line) and $FPI-SP$ (dashed line) algorithms. Signals: pressure $h(t)$ and pressure setpoint h_{sp}, flow discharge at the valve site $Q(t)$, valve closure $\alpha(t)$.

Due to the complex topology, the distributed nature of the WDN and the pressure dependent outflow from the demanding nodes, the local behaviour of the system may be changing a lot when considering different working points, not just in the static gain, but in a more complex and unpredictable way. For these reasons, the robustness of the RTC algorithms is of fundamental importance and should be tested around different working points. As an example, let us repeat the analysis at a working point characterised by a higher average of the total demand (let denote the related models with apex hf). The identification data and the model prediction are reported in Figure 15a. The Bode diagram of $\tilde{G}_{ah}^{hf}(s)$ is depicted in Figure 15b. The loop functions $\tilde{L}^{hf}(s)$, associated to the two control algorithms, are reported in the same Figure. The Bode criterion can be used to prove $FPI-SP$ stability while, in the case of the PI algorithm, the Bode diagram of $\tilde{L}^{hf}(s)$ crosses the 0 dB axis many times, thus contradicting one of the hypotheses required by the criterion. Stability of the PI algorithm must be therefore discussed from the Nyquist plot of the associated loop function, which is reported in Figure 14b, and highlights that the algorithm leads to instability around the considered working point. When considering the Nyquist plot of $FPI-SP$ loop function it is possible to understand how the algorithm is still stable, even if closer to the instability condition. Figure 16 shows a simulation of the WDN around the working point with higher total demand, with both control algorithms. As expected from the analysis, the PI algorithm leads to instability: note

how the speed of the PCV is always saturated during control. On the contrary, the $FPI - SP$ algorithms is correctly working, even if some minor oscillations are generated in the service pressure.

Discussion of Results

The analysis performed with the two different case studies confirms that the low order linear model, originally used to design the regulators, is misleading in reproducing the dynamic behaviour of the plant at higher frequencies, due to the presence of many pronounced resonance peaks where the model instead shows a very small magnitude. This motivates the use of a higher order model that captures the multiple resonant behaviour of the plant and allows to properly analyse stability and robustness of the control design. The proposed analysis also suggests that the higher order model can be an useful tool to complement the regulator design phase. In fact, while the first order model requires a trial and error procedure for the tuning of the gain of the regulator, the higher order model allows to tune the regulator directly on the model. Moreover, a tuning process based on higher order models, describing the process around different operating points, allows to provide stability and robustness over a wide range of operating conditions. Finally, the higher order model allows to explain in depth the benefits of the $FPI - SP$ design, both in terms of robustness and improved control sensitivity.

Conclusion

This work focuses on the stability and robustness of RTC algorithms based on local, linear dynamical models of the WDS around the working point. The analysis suggests that the instability can be caused by the presence of multiple resonance conditions that may not be described by the model used in the design of the regulator, concurrently with a consistent nonlinearity of the gain of the process under control. When possible, it is therefore advisable to base the regulator design on higher order models, which better describe the dynamics of the process around the working point. In particular, a higher order model allows to understand the presence of non de-amplified closed-loop oscillations at various frequencies, which can affect stability in presence of gain uncertainty. The different resonance peaks in the open-loop transfer function $G(s)$ should be carefully considered in the design of the loop function $L(s)$ to properly evaluate stability, robustness and overall dynamic performances of the control algorithm. In case this is not possible, wide robustness margins must be provided in the design of the feedback system. For this purpose, it is shown that the introduction of a low-pass filter and a Smith Predictor can significantly improve the robustness of the control scheme, while, at the same time, help reducing the cost of control. It is also advisable to consider auxiliary working points characterised by different values of flow discharge and repeat the analysis to ensure stability and robustness even in critical situations. Finally, another possibility to robustify the design of the controller would be introducing a nonlinear compensation to handle the gain nonlinearity, or to adapt the controller gains according to the operating conditions of the plant by means of a nonlinear gain compensator, as suggested for instance in Janus and Ulanicki (2018). This is left as future work.

Appendix: Frequency Response of Linear Time Invariant Systems, Bode Diagrams and Nyquist Plots

Laplace Transform

Let f be a complex function of the real variable t. Let then $s = \sigma + j\omega \in C$ be a complex variable. If the function

$$F(s) = \int_0^{+\infty} f(t)e^{-st}dt \tag{32}$$

exists at least for some values of s, then it is called *Laplace transform* of $f(t)$.

Transfer Function

A generic linear time invariant dynamic system is described by the following state-space representation:

$$\begin{cases} \dot{x}(t) = Ax(t) + Bu(t) \\ y(t) = Cx(t) + Du(t) \end{cases} \tag{33}$$

where $x(t)$ are the system states, $u(t)$ are the system inputs and $y(t)$ the system outputs, with $x \in \mathbb{R}^n$, $u \in \mathbb{R}^m$ and $y \in \mathbb{R}^p$. The value of n is called *order* of the system.
Let $X(s)$, $U(s)$, $Y(s)$ be the Laplace transforms of states, inputs and outputs, respectively. Then the matrix

$$G(s) = C(sI - A)^{-1}B + D = \frac{\beta_\nu s^\nu + ... + \beta_1 s + \beta_0}{\alpha_\nu s^\nu + ... + \alpha_1 s + \alpha_0} \tag{34}$$

with $\nu \leq n$, is called *transfer function*. The roots of the denominator of $G(s)$ are called *poles*, while the roots of the numerator of $G(s)$ are called *zeros*. Associated to a transfer function, there exist several possible state space representations.

Frequency Response of Linear Time Invariant Systems and Bode Diagrams

Let $G(s)$ be the transfer function describing a linear, time invariant system. The *frequency response* of the system coincides with the complex function $G(j\omega)$, i.e. the restriction of the transfer function $G(s)$ to the points belonging to the non negative imaginary axis of the complex plane ($s = j\omega$, $\omega \geq 0$), excluding the points coinciding with the poles of $G(s)$.
The *Bode plot* allows to graphically represent the frequency response of a system, and consists of two curves relating magnitude and phase of $G(j\omega)$ to ω. Note that a logarithmic scale (base 10) is used for the abscissa of both plots, while the magnitude of the frequency response is typically expressed in decibel (dB), as

$$|G(j\omega)|_{dB} = 20 \log_{10} |G(j\omega)| \tag{35}$$

The frequency response allows to study the response of the system to sinusoidal inputs. In particular, if $G(s)$ is an asymptotically stable system and $u(t) = Usin(\omega_0 t)$ is a sinusoidal input, then the steady-state output is given by $y(t) = |G(j\omega_0)|Usin(\omega_0 t + argG(j\omega_0))$.

Nyquist Plots

Let $G(s)$ be the transfer function describing a linear, time invariant system. The *Nyquist path* is the closed curve in the s plane composed of the imaginary axis and a half-circumference of infinite radius belonging to the right half-plane. The *Nyquist plot* is then the image through $G(s)$ of the Nyquist path, and is a closed curve in the complex plane, oriented according to increasing values of ω. Note that, in presence of poles of $G(s)$ with null real part, the Nyquist path is modified to encircle such poles with half-circumferences of infinitesimal radius, belonging to the right half-plane.

Data Availability Statement

All data, models, or code generated or used during the study are available from the corresponding author by request.

References

Campisano, A., Creaco, E., and Modica, C. (2009). Rtc of valves for leakage reduction in water supply networks. *Journal of Water Resources Planning and Management*, 136(1):138–141.

Campisano, A., Modica, C., Reitano, S., Ugarelli, R., and Bagherian, S. (2016). Field-oriented methodology for real-time pressure control to reduce leakage in water distribution networks. *Journal of Water Resources Planning and Management*, 142(12):04016057.

Campisano, A., Modica, C., and Vetrano, L. (2011). Calibration of proportional controllers for the rtc of pressures to reduce leakage in water distribution networks. *Journal of Water Resources Planning and Management*, 138(4):377–384.

Ciaponi, C., Franchioli, L., Murari, E., and Papiri, S. (2015). Procedure for defining a pressure-outflow relationship regarding indoor demands in pressure-driven analysis of water distribution networks. *Water resources management*, 29(3):817–832.

Creaco, E. (2017). Exploring numerically the benefits of water discharge prediction for the remote rtc of wdns. *Water*, 9(12):961.

Creaco, E., Campisano, A., Franchini, M., and Modica, C. (2017). Unsteady flow modeling of pressure real-time control in water distribution networks. *Journal of Water Resources Planning and Management*, 143(9):04017056.

Creaco, E., Campisano, A., and Modica, C. (2018). Testing behavior and effects of prvs and rtc valves during hydrant activation scenarios. *Urban Water Journal*, 15(3):218–226.

Creaco, E. and Franchini, M. (2013). A new algorithm for real-time pressure control in water distribution networks. *Water Science and Technology: Water Supply*, 13(4):875–882.

Farley, M. and Trow, S. (2003). *Losses in water distribution networks*. IWA publishing.

Fontana, N., Giugni, M., Glielmo, L., Marini, G., and Verrilli, F. (2017a). Real-time control of a prv in water distribution networks for pressure regulation: Theoretical framework and laboratory experiments. *Journal of Water Resources Planning and Management*, 144(1):04017075.

Fontana, N., Giugni, M., Glielmo, L., Marini, G., and Zollo, R. (2017b). Real-time control of pressure for leakage reduction in water distribution network: Field experiments. *Journal of Water Resources Planning and Management*, 144(3):04017096.

Galuppini, G., Creaco, E., Toffanin, C., and Magni, L. (2019). Service pressure regulation in water distribution networks. *Control Engineering Practice*, 86:70–84.

Janus, T. and Ulanicki, B. (2017). Hydraulic modelling for pressure reducing valve controller design addressing disturbance rejection and stability properties. Elsevier.

Janus, T. and Ulanicki, B. (2018). Improving stability of electronically controlled pressure-reducing valves through gain compensation. *Journal of Hydraulic Engineering*, 144(8):04018053.

Lambert, A., Fantozzi, M., and Thornton, J. (2013). Practical approaches to modeling leakage and pressure management in distribution systems–progress since 2005. In *Proceedings of the 12th Int. Conf. on Computing and Control for the Water Industry-CCWI2013*.

Ljung, L. (1991). *System identification toolbox: for use with MATLAB: user's guide*. Math Works.

Magni, L. and Scattolini, R. (2014). *Advanced and multivariable control*. Pitagora.

Morari, M. and Zafiriou, E. (1989). *Robust process control*. Prentice-Hall International Editions.

Pezzinga, G. (2000). Evaluation of unsteady flow resistances by quasi-2d or 1d models. *Journal of Hydraulic Engineering*, 126(10):778–785.

Prescott, S. L. and Ulanicki, B. (2008). Improved control of pressure reducing valves in water distribution networks. *Journal of hydraulic engineering*, 134(1):56–65.

Seborg, D. E., Mellichamp, D. A., Edgar, T. F., and Doyle III, F. J. (2010). *Process dynamics and control*. John Wiley & Sons.

Streeter, V. L., Wylie, E. B., and Bedford, K. W. (1998). Fluid mechanics, wcb.

Thornton, J. and Lambert, A. (2006). Managing pressures to reduce new breaks. *Water*, 21(December 2006):24–26.

Ulanicki, B. and Skworcow, P. (2014). Why prvs tends to oscillate at low flows. *Procedia Engineering*, 89:378–385.

Walski, T. M., Chase, D. V., Savic, D. A., Grayman, W., Beckwith, S., and Koelle, E. (2003). Advanced water distribution modeling and management.

Zhou, K., Doyle, J. C., Glover, K., et al. (1986). *Robust and optimal control*. Prentice-Hall.